공학석사 학위논문

Multi-contrast imaging: a Novel Pulse Sequence for Simultaneous Acquisition of Proton Density, T_1-Weighted, T_2-Weighted and FLAIR Images

다중 컨트라스트 영상기법: Proton density, T_1, T_2 및 FLAIR 영상을 동시에 획득하는 펄스시퀀스

2017년 7월

서울대학교 대학원
전기·정보공학부
정 진 희

Multi-contrast imaging: a Novel Pulse Sequence for Simultaneous Acquisition of Proton Density, T_1-Weighted, T_2-Weighted and FLAIR Images

지도 교수 이 종 호

이 논문을 공학석사 학위 논문으로 제출함
2017년 7월

서울대학교 대학원
전기·정보공학부
정 진 희

정진희의 공학석사 학위논문을 인준함
2017년 7월

위 원 장 한 승 용 (인)

부위원장 이 종 호 (인)

위 원 오 세 홍 (인)

Abstract

Magnetic Resonance Imaging (MRI) is a widely used non-invasive clinical imaging modality. Unlike other medical imaging tools, such as X-rays or computed tomography (CT), the advantage of MRI is that it uses non-ionizing radiation. In addition, MRI can provide images with multiple contrasts by using different pulse sequences and protocols. However, image acquisition speed is known to be a major drawback of MRI and is a limitation in various MRI applications.

To address speed limitations in acquisition of multiple contrasts images, we developed a new pulse sequence called Multi-contrast sequence that enables simultaneous acquisition of the four contrasts images, proton density (PD), T_1-weighted, T_2-weighted and FLAIR images, with a single scan in less than 6 min. Multi-contrast sequence is a combination of fast spin-echo (FSE) based imaging pulse sequences with inversion recovery (IR) acquisition and non-IR acquisition. From Multi-contrast sequence, two contrasts of fluid-attenuated images, PD images, and T_2-weighted images are acquired at the same time and T_1-weighted images are synthesized from the obtained images. Compared to conventional imaging sequences, the scan time is reduced by 50 %. Additionally, the new method generates both T_1 maps and T_2 maps that can be used for quantitative imaging.

To demonstrate the effectiveness of our approach, phantom and in vivo experiments are performed. Then signal to noise ratio (SNR) of images from the proposed sequence and from the conventional sequences are compared. The method may have potentials as a rapid evaluation tool for clinical scans.

Keyword : Magnetic resonance imaging, multi-contrast, fast spin-echo, FLAIR image, quantitative imaging
Student Number : 2015 - 20990

Table of Contents

List of Tables

List of Figures

1. Introduction

1.1. Principles of MRI

Magnetic resonance imaging (MRI) is a technique utilized for diagnostic purpose based on the phenomenon of nuclear magnetic resonance (NMR). The dominant nucleus in MRI applications is the hydrogen nuclei (proton), and most MR imaging techniques are based on resonance effects of protons. Hydrogen protons are similar to small satellites, and they consistently rotate around the axis as if the earth is rotating, which means that the hydrogen nuclei have a spin. At this time, a positive electric charge is attached to the hydrogen nucleus and rotates about the axis, and a current is generated due to the nuclear spin of the positively charged hydrogen. When there is a current flow, a magnetic field is generated. The direction and intensity of the formed magnetic field are expressed as a vector, which is called a Nuclear Magnetic Moment.

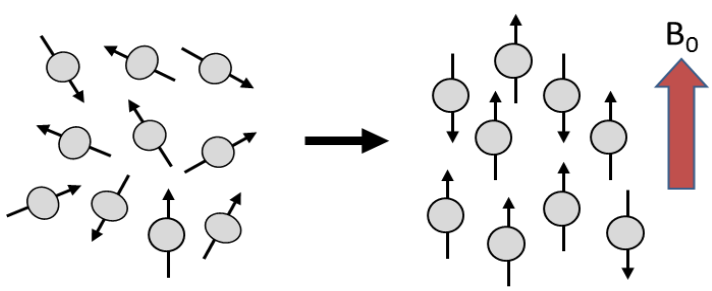

Figure 1. Pictures of a collection of protons. In the absence of an external magnetic field, the protons are randomly oriented. However, inside a magnetic field, they are aligned parallel to or opposite to the magnetic field.

When the protons are in a state without an external magnetic field, the direction of spin vectors is randomly arranged. Therefore, the net magnetization (M_0) defined by the vector sum of spins vectors become zero. When the spins are exposed in an external static magnetic field (B_0), two phenomena are observed. First, the spins

are arranged in two directions parallel to or opposite to the external magnetic field. The vector sum of spins aligned in opposite direction is canceled out and net magnetization is formed by the vector sum of the remaining spins. Second, the rotation axis of spins rotates around the B_0, which is called precession. The precession frequency, also known as Larmor frequency, is proportional to the strength of the external magnetic field and defined as the following equation [1]:

$$\omega_0 = \gamma B_0 \qquad (1.1)$$

where, $\omega_0$is the precession frequency and γ is the gyromagnetic ratio. For hydrogen, the gyromagnetic ratio is $\gamma/2\pi$ = 42.58MHz/T. The strength of B_0 is expressed in Tesla (1T = 10,000 Gauss).

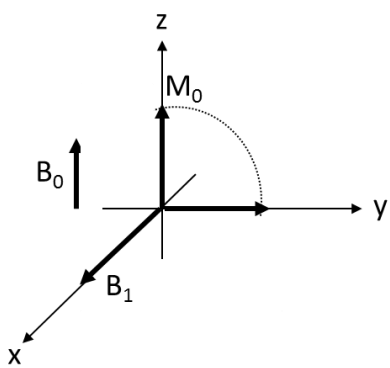

Figure 2. Excitation. B1 RF field tuned to precession frequency and applied along the x axis rotates the net magnetization vector on the z axis to be placed on the transverse plane (x-y plane).

To obtain the signals from the protons, the net magnetization arranged in the direction of the magnetic field (vertical axis) must be moved in the transverse direction. To flip the net magnetization from vertical axis to transverse direction, a radio frequency (RF) pulse with frequency range tuned to precession frequency is applied and this process is called excitation. Once the spins are excited, the phase of spins changes from out of phase to in phase. Hence, the magnetization of the longitudinal axis disappears and new magnetization of the transverse axis is generated by the resonance phenomenon. The RF pulse is sometimes referred to as B_1 and the

magnetic field experienced by spins is B as follows:

$$B = B_0 + B_1 \qquad (1.2)$$

When the spins are excited and RF is turned off, the spins will spontaneously emit energy and eventually return to its initial state. This process of returning to the initial state is called relaxation. During the relaxation process, the transverse magnetization disappears and the longitudinal magnetization returns to the initial net magnetization. The relaxation rate is different for different tissue types and there are two typical time constants (T_1 and T_2) that characterize the relaxation process. T_1 represents the relaxation rate of longitudinal magnetization and T_2 represents the relaxation rate of transverse magnetization. The overall effects described above can be combined in a differential equation that explains the behavior of magnetization in MRI. The formulation is known as the Bloch equation [2]:

$$\frac{dM}{dt} = (M \times \gamma B) - \frac{(M_x\hat{x} - M_y\hat{y})}{T_2} - \frac{(M_z - M_0)\hat{z}}{T_1} \qquad (1.3)$$

where $\mathrm{M} = [M_x\, M_y\, M_z]^T$ is the magnetization vector, $\hat{x}, \hat{y},$ and $\hat{z}$ denotes a unit vector in the *x, y, z* directions respectively, B is the total magnetic field, and T_1 and T_2 are the relaxation times.

1.2. Pulse sequence

In MRI, pulse sequence is a series of combination of RF pulses and gradient fields and can be used to generate a signal from hydrogen protons. Theoretically any kinds of RF pulse and gradient combinations are possible and can make different signal intensity and image contrasts. A variety of sequences are used in clinical practice, and the most frequently used is spin echo (SE) sequence [3]. A pulse sequence of SE is depicted in Figure 3. After applying excitation RF pulse for flipping the magnetization on longitudinal axis into the transverse plane, a refocusing RF pulse is used to

rephase the dephasing spins and eventually leads to a new alignment of all spins. This newly aligned magnetization is called an echo.

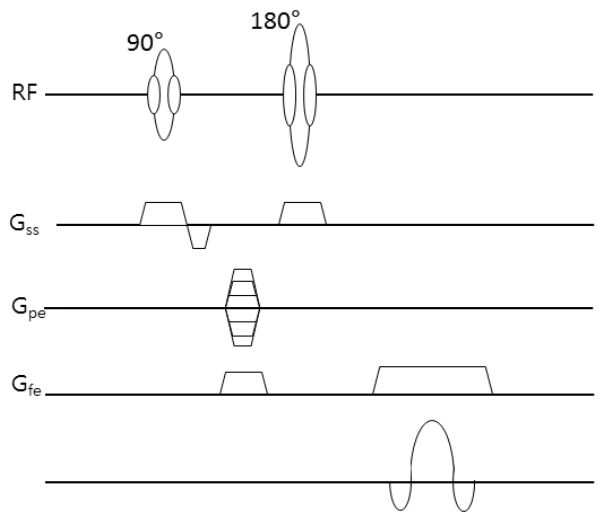

Figure 3. Pulse sequence of spin echo

Typically, excitation RF pulse is also referred to as 90° pulse and refocusing RF pulse is referred to as 180° pulse. There are three kinds of gradient fields; slice selection gradient (G_{ss}), phase encoding gradient (G_{pe}), frequency encoding gradient (G_{fe}). The time between the center of excitation pulse and the center of the echo is called an echo time (TE). This pulse sequence is repeated with a time delay, which is referred to as the repetition time (TR). That is the time between the center of excitation pulse and the center of next excitation pulse is TR. Multiple refocusing RF pulses can be applied to make more echoes as introduced in [36]. As shown in Figure 4, a pulse sequence with multiple refocusing pulses is called fast spin echo (FSE). Because FSE acquires multiple echoes within a TR, it can scan within a shorter time than SE sequence.

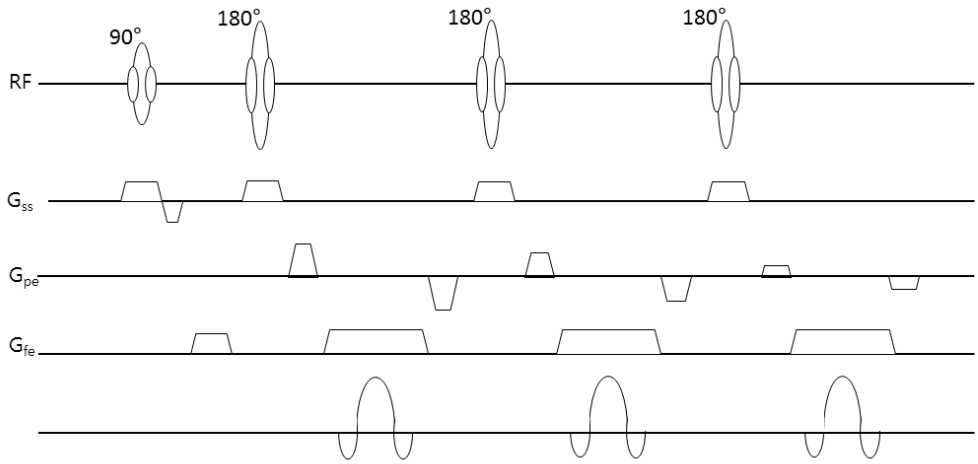

Figure 4. Pulse sequence of fast spin echo

1.3. Contrast Mechanisms

In 1970s, it was discovered that there was significant difference of the T1 and T2 values between tumor tissue and normal tissue [4]. Usually many disease changes the quantities of tissue parameters, and common diagnostic methods observe the values from particular tissue of interest. So, many various types of measurement pulse sequences have been developed to make different kinds of contrast in images and the quantity estimation of tissue parameters on region of interest (ROI) is possible thereby. Figure 5 shows an example of contrasts.

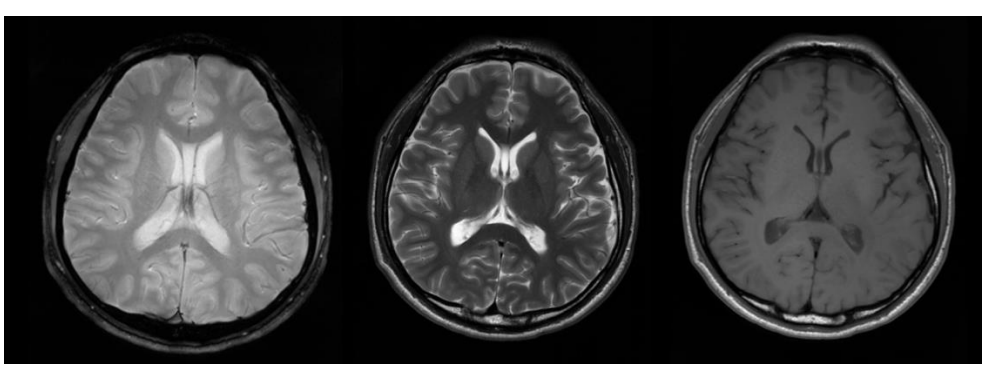

Figure 5. Different image contrasts. (Left) Proton density weighted contrast, (middle) T_2-weighted contrast, and (right) T_1-weighted contrast.

Proton density (PD) image has proton density weighted contrast with a contrast ratio proportional to the number of proton of the tissue in a certain range of a patient. So the overall signal intensity of PD image is high and it is mainly used to observe a wide range of tissue. To obtain a PD image, TE should be the minimum value achievable, and a long TR value should be chosen to make sure that maximum magnetization is recovered from each RF excitation. T_2-weighted contrast can be achieved by increasing TE and TR. Because the magnitude of signal loss depends on T_2 relaxation time constant during the TE, the signal loss is larger in regions with a short T_2 value than in regions with a long T_2 value. T_2-weighted image easily represents characteristic change of a tissue and very useful for tumor identification. Clinically, T_1-weighted images are mainly used to observe anatomical structure. In order to obtain an accurate T_1-weighted image, the data of the image must be received without the T_2 relaxation effect. So, T_1-weighted contrast is acquired by using a short TE and a short TR

1.4. Image Formation

A signal generated after an excitation is called echo signal. When spins are excited by applying an RF pulse to an MRI having a magnetic field strength B_0, the echo signals with the same precession frequency are received regardless of the position of the slice to be imaged. If all echo signals from the whole body have the same precession frequency, all the signals are summed together, and it is impossible to distinguish which signal comes from which position. However, if only one slice of body is excited and position information of up, down, left and right in the slice is given, the image of the slice can be constructed by using the position information from the received signal later. In MRI, a 3D spatial coordinate system is used. The same direction as B_0 is referred to as a z-axis and slice selection gradient is used to set the position information on the z-axis. In the selected slice, vertical direction is defined as a y-axis and horizontal direction is defined as an x-axis,

and then a phase encoding gradient and a frequency encoding gradient are used to set the position information on the y-axis and the x-axis.

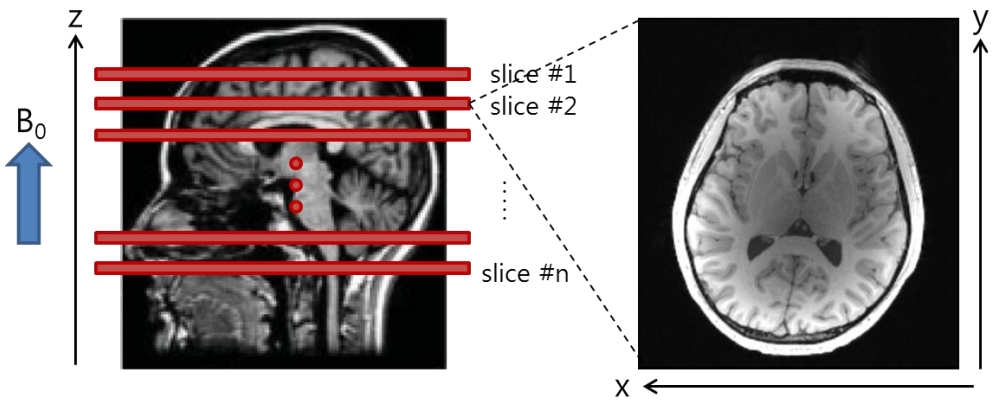

Figure 6. Image formation. To specify the position information in the 3D spatial coordinate system, slice selection, phase encoding and frequency encoding gradients are used. Slice selection gradient is used to set the position information on the z-axis (longitudinal direction which is the same direction as B_0). In the selected slice, vertical and horizontal directions are defined as y-axis and x-axis, respectively. Then a phase encoding gradient and frequency encoding gradient are used to set the position information on the y-axis and x-axis, respectively.

An echo signal with spatial coordinate information using three gradients is digitized by sampling process. The digitized data is called raw data and the space filled with these raw data is called *k*-space.

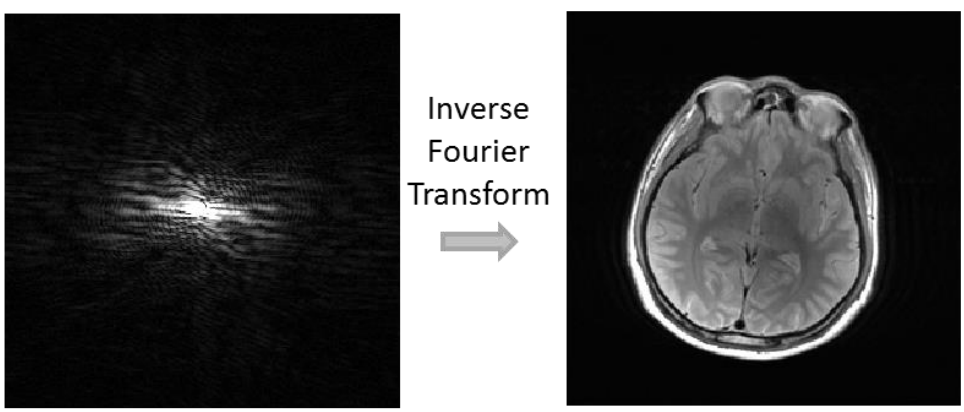

Figure 7. Echo signal are sampled and stored in *k*-space. A raw data in *k*-space (left) is transformed into an image (right) by inverse Fourier Transform.

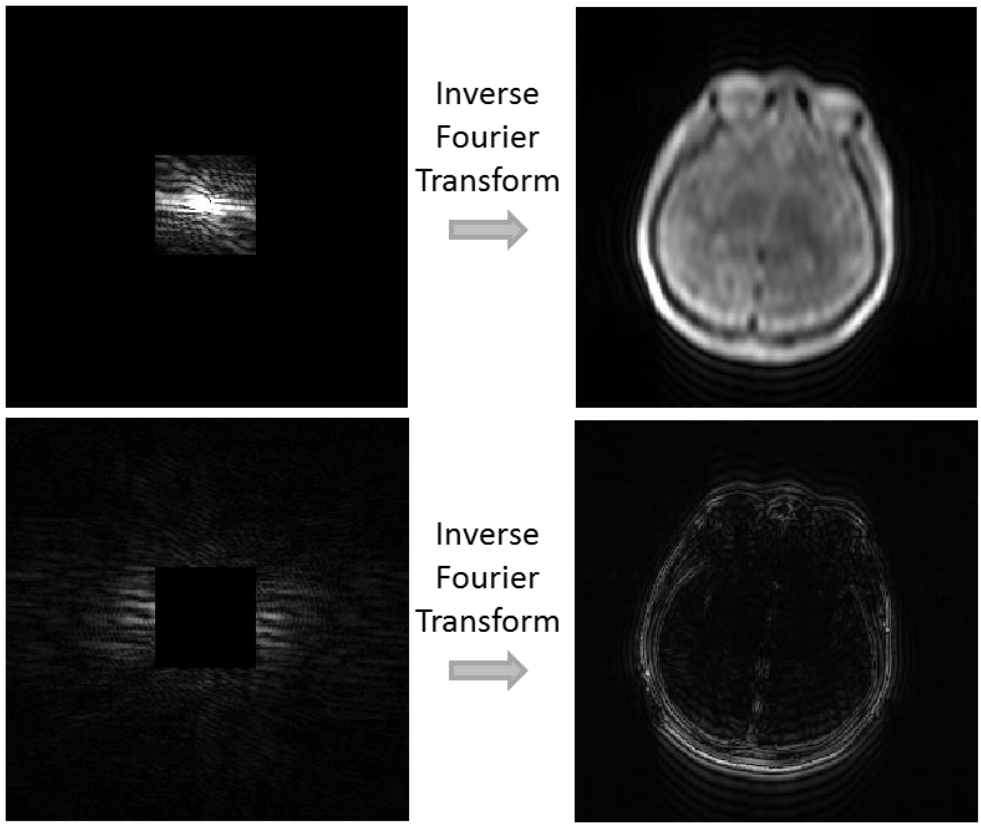

Figure 8. Characteristic of *k*-space. (Top row) The signal obtained at the center of the *k*-space is mainly involved in the contrast of an image. (Lower row) the signal at the edge of *k*-space shows a detailed description or a boundary between tissues in an image.

After all *k*-space have been filled, inverse Fourier transform is performed to obtain the actual image. As shown in Figure 7, the signal intensity obtained at the center of the *k*-space is high and the edge of the *k*-space has low signal intensity. A point in *k*-space is not directly mapped to a point in an image. One point in *k*-space has magnetization information of all points in an image. Figure 8 shows the characteristics of *k*-space according to the position and its effect on an image. As in the case of the top row, if only the data in the center region of k-space is cropped and converted to an image, the resulting image has a contrast but blurry. As shown in the row below, if only the data in the edge region of the k-space is converted to an image, the resulting image has sharp edges but low contrast. The signal obtained at the center of *k*-space is mainly

involved in the contrast of an actual image. On the other hand, the signal at the edge of the k-space mainly shows a detailed description or a boundary between tissues in an image.

1.5. Quantitative MRI

T_1 relaxation time constant is one of MR quantitative parameters. The process in which magnetization of longitudinal axis is recovered to its initial state after excitation is referred to as relaxation or longitudinal relaxation. The longitudinal relaxation is also called spin-lattice relaxation because it transfers the energy of hydrogen nuclei to the surrounding material (lattice). The time until the magnetization of longitudinal axis is recovered to about 63% of the initial magnetization after an excitation is defined as of T_1 relaxation time constant of a given material. The typical method for T_1 value measurements is using a series of inversion recovery, which consists of an inversion pulse that inverts the initial longitudinal magnetization on the z axis into the opposite z-direction. After that, an excitation pulse is applied with different time delays following the inversion pulse. Then, the excitation pulse flips the longitudinal magnetization recovered after the time delay and causes an MR signal. Because the strength of signal is dependent on T_1 value, T_1 relaxation time constant can be obtained by fitting process from repeatedly acquired signals for different time delays. The phase of spins immediately after an excitation is in-phase. As time goes on, the spins on the isotope is scattered in the transverse plane due to the interaction of spin and spin. This is called dephasing, and the more diphase is, the smaller the MR signal becomes. The decrease of the MR signal due to the interaction between spins is called T_2 relaxation and it is called transverse relaxation or spin-spin relaxation. The T_2 relaxation time constant of a given substance is defined as the time until the transverse magnetization reaches 37% of initial magnetization, and is always below T_1 relaxation time constant. T_2 relaxation time constant can be measured by pixel by pixel fitting a series of data with different

TEs to exponential curve. To acquire images with different TEs, multi-echo spin echo sequence is commonly used. The T1 and T2 time constant values for the variety of measured tissues are presented in Table 1 [5].

Table 1. T_1 and T_2 relaxation times at 3T and 1.5T.

Tissue	3T		1.5T	
	T_2 [ms]	T_1 [ms]	T_2 [ms]	T_1 [ms]
Liver	42±3	812±64	46±6	576±30
Muscle	50±4	1412±13	44±6	1008±20
Kidney	56±4	1194±27	55±3	690±30
White matter	69±3	1084±45	72±4	778±84
Gray matter	99±7	1820±114	95±8	1086±228
Blood	275±50	1932±85	290±30	1441±120

2. Multi-contrast sequence

2.1. Introduction

MRI is a widely used medical imaging modality that forms images of anatomy with various soft-tissue contrasts and the physiological processes of the body. Although multiple contrast images provide diagnostically valuable information, long scan time required for the multiple contrast images is the major limitation of MRI, particularly when considering lengthy acquisition time in clinical protocols. Moreover, in certain applications, tissue parametric maps (e.g. PD, T_1 and T_2 maps) are acquired to measure pathology quantitatively or to observe longitudinal signal changes quantitatively. These parametric mapping methods also require additional scan time because of repetitive acquisitions of multiple TRs and TEs.

In order to reduce the data acquisition time, several techniques have been proposed. One of these techniques is to decrease the amount of k-space data collected. The partial Fourier techniques [8],[9] were used to reconstruct an entire MR image from only a part of k-space data by utilizing conjugate symmetry property of MR signal. Parallel MR imaging techniques [10]~[13] were able to achieve acceleration of data acquisition by taking advantage of the inherent spatial sensitivity information from phased-array radiofrequency coils. In addition, sampling along a non-Cartesian trajectory [14]~[17] can also reduce the scan time by maximizing the efficiency of MR gradient hardware for the rapid coverage of k-space. MR imaging techniques based on compressed sensing (CS) theory and random sampling scheme were introduced to reconstruct MR image from highly undersampled data and therefore provide acceleration of acquisition speed [18],[19]. While these approaches are possible to increase data acquisition speed, it is considerably more complex to reconstruct images from non-Cartesian data and/or from undersampled data. Furthermore, reconstruction of

missing data requires additional information such as coil sensitivity maps or autocalibration information (ACS) to remove aliasing artifacts. Also, reconstructing images from undersampled data commonly associated with a penalty in the signal-to-noise ratio (SNR).

Instead of decreasing the amount of k-space data collected for improvements in acquisition time, a number of methods that acquire multiple contrast images in a single scan have been proposed. Fast spin echo (FSE) sequence employing k-space data sharing between images of different contrasts is proposed for dual-contrast or triple-contrast FSE sequence [20],[21]. Dual contrast gradient spin-echo (GRASE) [22], triple-contrast TSE acquisition [23] and 2in1-RARE [24] are multi-contrast acquisitions without k-space data sharing method. Because inversion time of fluid-attenuated inversion recovery (FLAIR) image for cerebral spinal fluid (CSF) suppression increases scan time substantially, FASCINATE [25] and dual-echo fast FLAIR [26] are introduced for acquisition of FLAIR image simultaneously with other contrast images. In a three-dimensional scan, [27] and [28] were proposed because additional slice encoding process leads to an increase of scan time. Despite these improvements in acquisition speed, typically only two or three contrast images are acquired in a single scan using each technique.

In MR quantitative mapping, to reduce the scan time for quantitative imaging, various studies have been introduced. Recently, magnetic resonance fingerprinting (MRF) [32] has received much attention. The basic idea of MRF is to first acquire the tissue parameters like T_1 and T_2 in a short time using random sampling and CS theory and then generate T_1-weighted and T_2-weighted images based on them. Although scan time can be shortened, the accuracy of the calculated tissue parameters has not been verified, and there is a problem that the images created based on these tissue parameters are artificial. Especially when there are substances with multicomponent T_1 or T_2 values in a single voxel, it is difficult to obtain the exact T_1 or T_2 value from fitting process.

Therefore there is still a limitation to use MRF in clinical practice, and a method of obtaining diagnosis-ready images and quantitative images at the same time is proposed [33].

The purpose of this study is to propose a novel pulse sequence that enables simultaneous acquisition of the four contrast images (PD, T_1, T_2, FLAIR) in less than 6 min. These four images are most frequently used in clinical practice. So reducing the time to obtain these images is a significant contribution to improving the workflow of the patient diagnosis process. In addition to the four contrast images, the proposed method also provides T_1 and T_2 maps. With proposed pulse sequence, it is possible to calculate T_1 and T_2 maps because two pair of images with the same TR and different TE and with the same TE and different TI are obtained. To demonstrate the effectiveness of our approach, phantom and in vivo experiments are performed. The method may have potentials as a rapid evaluation tool for clinical scans.

2.2. Materials and Methods

2.2.1. Design of Multi-contrast sequence

To acquire fluid-attenuated images, inversion recovery (IR) acquisition is commonly used. In inversion recovery acquisition [6], inversion pulse with a flip angle of θ_{inv} is applied to the slice to be scanned to invert the magnetization of the slice and the scan is performed when the magnetization of CSF is recovered to zero. The time taken for the magnetization of CSF to become zero after the inversion pulse is applied is called time of inversion (TI). If the inversion pulse is applied and the slice is excited after the TI, the tissue other than the CSF has magnetization of any size recovered during the TI, but since the magnetization of the CSF is zero, a fluid-attenuated image with a dark CSF region is obtained. For FSE, TI is calculated in proportion to TR as follows:

$$TI_{flair} = T_1[ln\,2 - ln(1 + e^{-(TR-TE_{last})/T_1})] \qquad (2.1)$$

At 3T, TI usually required a long time of about 2500 *ms*. Since the IR module consisting of the inversion pulse, the slice-selection gradient (G_{ss}), and the spoiler takes only a short time compared to the long TI, the remaining time after IR module time from TI is maintained as an idle time. In case of multi-slice scan, interleaved IR acquisition [34] is applied rather than sequential IR acquisition in order to shorten the scan time by utilizing the idle time. In sequential IR acquisition case, the data is acquired after TI from IR module, and this process is sequentially performed on a slice-by-slice basis. On the other hand, in interleaved IR acquisition case, the idle time for an arbitrary slice is utilized to play out IR modules for other slices. So, interleaved IR acquisition is more time-efficient than sequential IR acquisition and commonly preferred when TI is long.

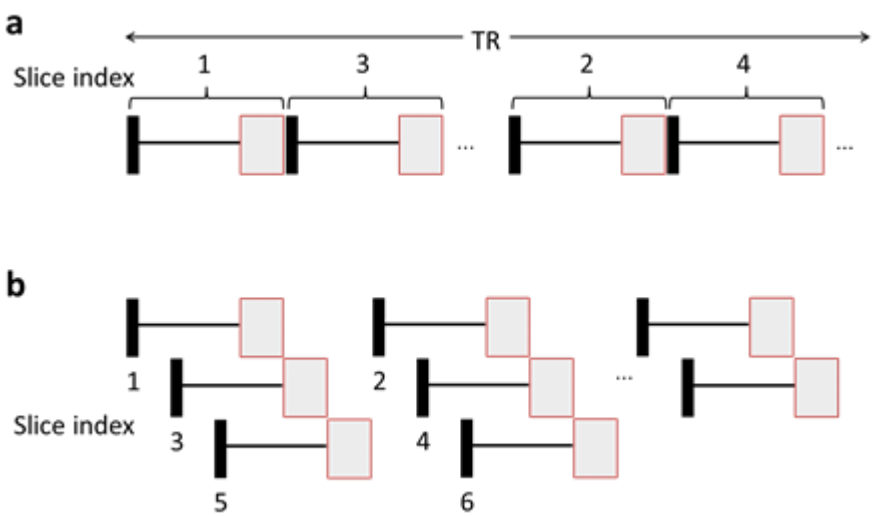

Figure 9. IR acquisition schemes for FLAIR imaging: (a) sequential IR acquisition, (b) interleaved IR acquisition. The black boxes and the red boxes represent the IR module and the imaging pulse sequence, respectively. The solid line connecting the two boxes represents the inversion time.

The Multi-contrast sequence obtains all four contrast images. After applying the inversion pulse, two contrast images with short TE and long TE are acquired and two contrast images with short

TE and long TE without applying inversion pulse are acquired. From IR acquisition, the image with short TE (PD-FLAIR contrast image) and the image with long TE (T_2-FLAIR contrast image) are obtained. From non-IR acquisition which does not use an inversion pulse, the image with short TE (PD contrast image) and the image with long TE (T_2-weighted contrast image) are obtained. In the Multi-contrast sequence, the whole slice is divided into two groups, an odd numbered slice group and an even numbered slice group and the interleaved IR acquisition method is applied to each group to obtain a fluid-attenuated image. First, both PD-FLAIR and T_2-FLAIR contrast of odd numbered slice group and PD and T_2-weighted contrast of even numbered slice group are simultaneously acquired. Then PD-FLAIR and T_2-FLAIR contrast of even numbered slice group and PD and T_2-weighted contrast of odd numbered slice group are simultaneously acquired.

The schematic and timing diagram of the proposed Multi-contrast pulse sequence is illustrated in Figure 10. Imaging pulse sequence employing inversion RF pulse and imaging pulse sequence with non-IR acquisition are combined into single sequence in time-efficient way. IR module and the associated imaging pulse sequence for fluid-attenuated images of the odd slices are applied and the imaging pulse sequence for PD and T_2-weighted images of the even slices is inserted in a part of the TI. After the magnetization of the even slices is recovered, then the IR module and the associated imaging pulse sequence of even slices are applied. Similarly, the imaging pulse sequence for PD and T_2-weighted images of odd slices is inserted at the idle time after IR module for even slices during TI. In this way, Multi-contrast pulse sequence of even and odd slice groups are designed in interleaved order to obtain PD-FLAIR and T_2-FLAIR images through IR acquisition and PD and T_2-weighted images through non-IR acquisition at idle time of TI.

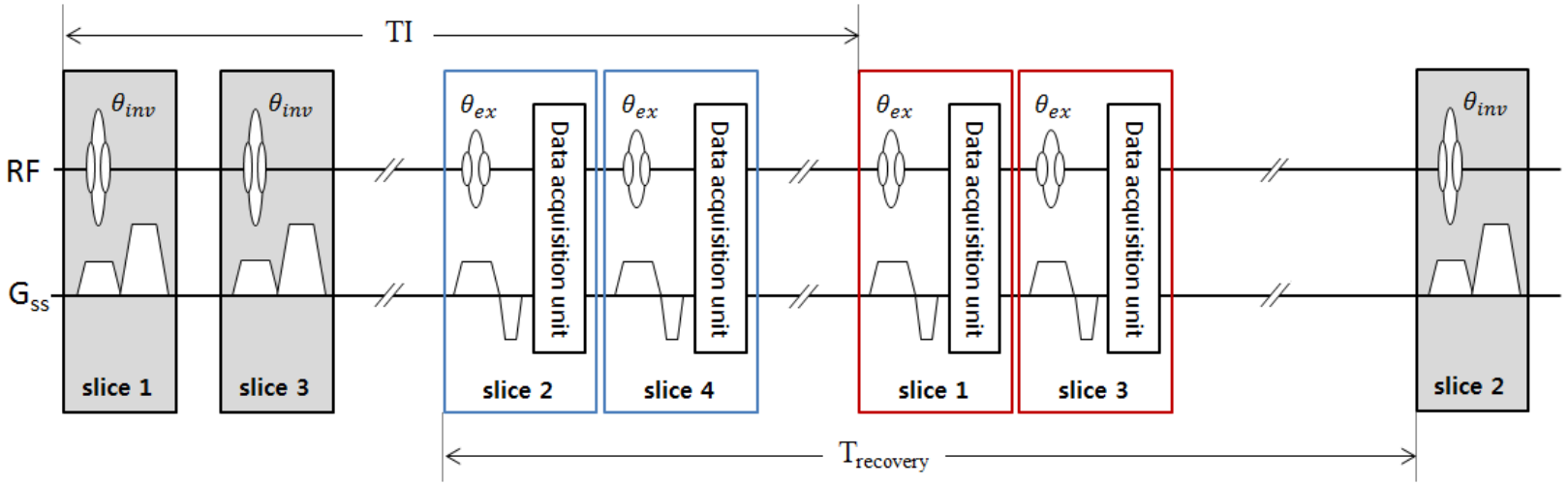

Figure 10. A schematic of the proposed pulse sequence: Imaging pulse sequence employing inversion pulse and imaging pulse sequence with non-IR acquisition are combined into single sequence in time-efficient way. The gray box denotes IR module and the red box denotes imaging pulse sequence of acquiring fluid-attenuated images after inversion time from the associated IR module. The blue box denotes imaging pulse sequence for non-IR acquisition.

Figure 11 shows a schematic of multi-slice scan. During the first part of a repetition time (TR) the scanner plays out a series of IR modules and imaging pulse sequences for PD-FLAIR and T_2-FLAIR images of odd slices. PD and T_2-weighted images of even slices are acquired at the idle time of TI for odd slices. After a recovery time ($T_{recovery}$, a time between the excitation RF pulse and the inversion RF pulse in the following acquisition block) of even slices, IR module and imaging pulse sequences for PD-FLAIR and T_2-FLAIR images of even slices are executed during a later part of the same TR interval. Similarly, PD and T_2-weighted images of odd slices are acquired at the idle time of TI for even slices. Thus, a TR can be expressed as follows:

$$TR = TI + 2T_{recovery} \qquad (2.2)$$

$T_{recovery}$ is the time between excitation and inversion pulse, during which the magnetization of excited slices is recovered and inverted by the following inversion pulse. The inversion time of Multi-contrast sequence was calculated by the following equation. Unlike the calculated TI of equation (2.1) for conventional FLAIR sequence, TI of Multi-contrast sequence was determined by $T_{recovery}$.

$$TI_{multi-contrast} = T_1 \, ln(2 - e^{-T_{recovery}/T_1}) \qquad (2.3)$$

The maximal number of slices that can be accommodated by a TI is given by the following equation.

$$N_{slice} = 2 * integer\ of \left(\frac{TI}{2 * time\ of\ imaging\ pulse\ sequence}\right) \qquad (2.4)$$

The timing of all sequence blocks was carefully designed for CSF saturation in FLAIR while acquiring full brain slices.

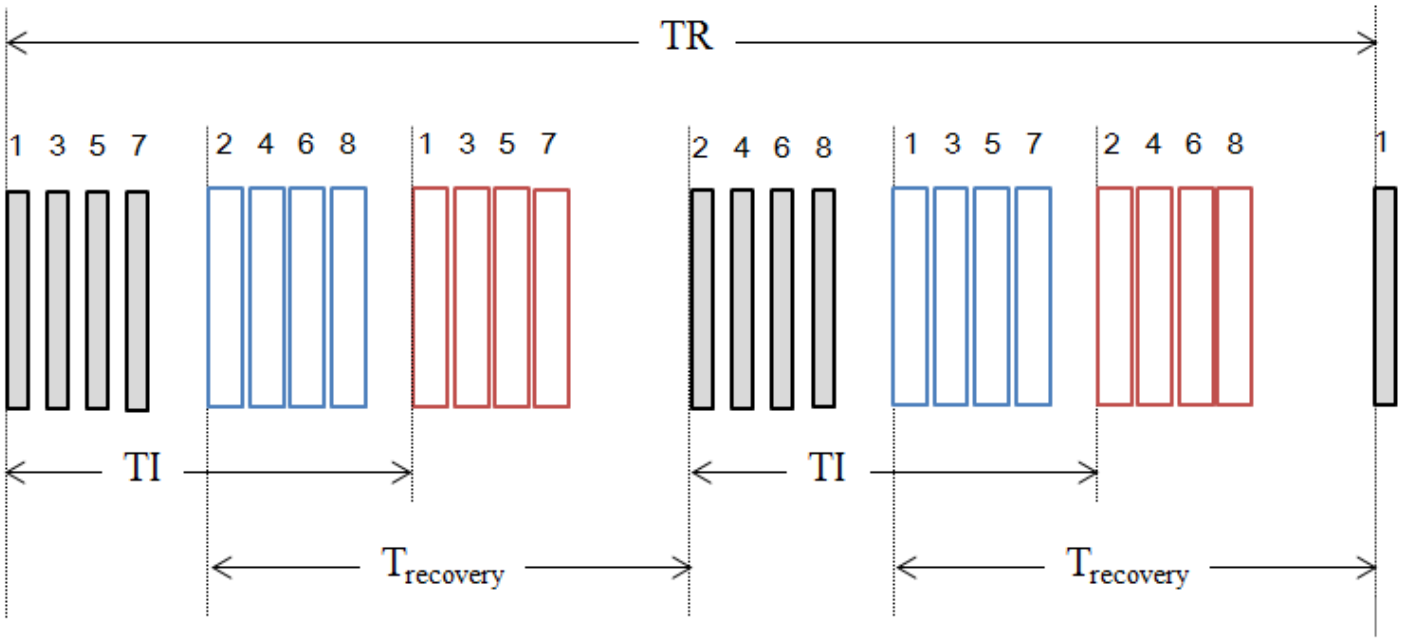

Figure 11. A schematic for multi-slice acquisition of Multi-contrast sequence. TI (inversion time) is a time interval between inversion RF pulse and the excitation RF pulse in imaging pulse sequence. $T_{recovery}$ is a time between the excitation RF pulse and the inversion RF pulse in the following acquisition block. TR is calculated as the sum of TI and twice of $T_{recovery}$.

To determine the inversion time for Multi-contrast sequence, we can track the time course of magnetization of z axis (M_z), as depicted in Figure 12

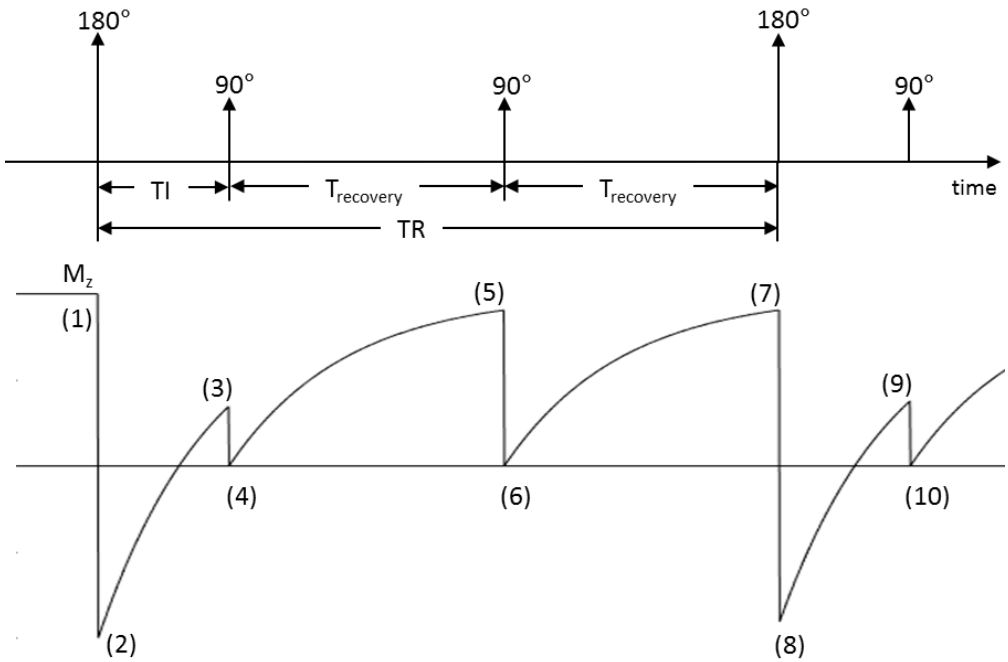

Figure 12. Time course of longitudinal magnetization for Multi-contrast sequence.

Referring to the number labels in Figure 12, the sequence of events is as follows:

1. Initial condition is at equilibrium:

$$M_z = M_0 \qquad (2.5)$$

2. The inversion excitation tips M_z from +z to –z:

$$M_z = -M_0 \qquad (2.6)$$

3. After a T_1 recovery time of TI, the magnetization grows to:

$$M_z = M_0(1 - 2e^{-TI/T_1}) \qquad (2.7)$$

4. The excitation pulse rotates the longitudinal magnetization into the transverse plane:

$$M_z = 0 \qquad (2.8)$$

5. The z−component recovers during the time $T_{recovery}$ to

$$M_z = M_0(1 - e^{-T_{recovery}/T_1}) \qquad (2.9)$$

6. The excitation pulse saturates the magnetization

$$M_z = 0 \qquad (2.10)$$

7. The z−component recovers during the time $T_{recovery}$ to

$$M_z = M_0(1 - e^{-T_{recovery}/T_1}) \qquad (2.11)$$

8. The refocusing pulse inverts the magnetization

$$M_z = -M_0(1 - e^{-T_{recovery}/T_1}) \qquad (2.12)$$

9. After the TI interval, the magnetization is recovered as:

$$M_z = M_0(1 - e^{-TI/T_1}) + [-M_0(1 - e^{-T_{recovery}/T_1})]e^{-TI/T_1} \qquad (2.13)$$

10. The excitation pulse tips the longitudinal component into the transverse plane and we have returned to state 4.

TI can be calculated by setting

$$1 - 2e^{-TI/T_1} + e^{-T_{recovery}/T_1}e^{-TI/T_1} = 0 \qquad (2.14)$$

We get

$$TI = T_1 ln(2 - e^{-T_{recovery}/T_1}) \qquad (2.15)$$

In this proposed sequence, dual-echo FSE (DE-FSE) sequence based on the Carr-Purcell-Meiboom-Gill (CPMG) pulse train was used as the imaging pulse sequence for both IR and non-IR acquisition to acquire two contrast images with short TE and long TE simultaneously. The pulse sequence of DE-FSE is shown in the Figure 13. The waveform of slice selection gradient was not shown for simplicity and the recusing RF pulse with flip angle θ_{ref} was simply represented by solid lines. Actually sinc RF pulse was used for refocusing pulse. For the implementation of the DE-FSE, the edges of k-space phase encoding lines were shared by two different effective echo time images to further reduce the scan time as introduced in [20]. Echo train length (ETL) for DE-FSE was 12 with the first 4 echoes and the latter 4 echoes were assigned to center-part of phase encoding lines of two images with short and long effective echo time, $T_{eff,short}$ and $T_{eff,long}$, respectively. In other words, phase encoding order was designed to set $T_{eff,short}$ equal to TE of the first echo of echo train and $T_{eff,long}$ equal to TE of the 11^{th} echo of echo train and the effective ETL of each image was 8. The rest 4 echoes from the center of ETL were assigned to edge-part of phase encoding lines and shared by the two images. The phase encoding order of shared echoes was designed to optimize the image with $T_{eff,long}$.

From the acquired four contrast images, T_1 weighted images were generated using the following equation as introduced in [29]. It is possible to obtain T_1 weighted images by dividing PD-FLAIR images by PD images, but because the noise in PD images may be amplified, the method in [29] is applied.

$$\frac{(PD\_FLAIR * PD)}{(PD\_FLAIR^2 + PD^2)} \qquad (2.16)$$

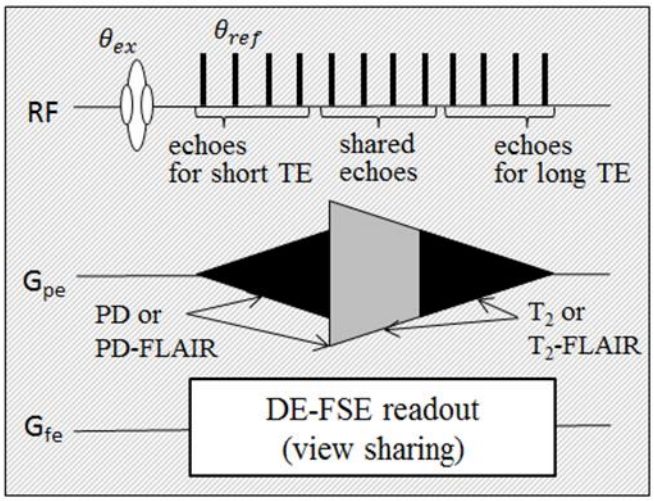

Figure 13. Data acquisition unit. Dual-echo FSE sequence with view sharing is used as the imaging pulse sequence for the acquisition of four contrast images.

2.2.2. Phantom development

The developed phantom, shown in Figure 14, consists of seven-tube containing water doped with a T_1-relaxation time constant modifier and a T_2-relaxation time constant modifier. $GdCl_3$ was used as the T_1-relaxation time constant modifier and agarose was used as the T_2-relaxation time constant modifier. Tube 1 was filled with oil and the other tubes were filled with water doped with $GdCl_3$ concentration of 32, 8, 8, 16, 16, 24 *ul*, and agarose concentration of 1.054, 0.525, 0.652, 0.82, 0.799, 0.4 *g*, corresponding to the tubes numbered 2 through 7. This phantom offered a T_1 range of 45 ~ 1300 *ms* and T_2 range of 80 ~ 280 *ms.* Tube 5 and 6 were filled with similar concentrations of T_1-relaxation time constant modifier and T_2-relaxation time constant modifier to verify consistency of T_1 and T_2 mapping result over different spatial locations.

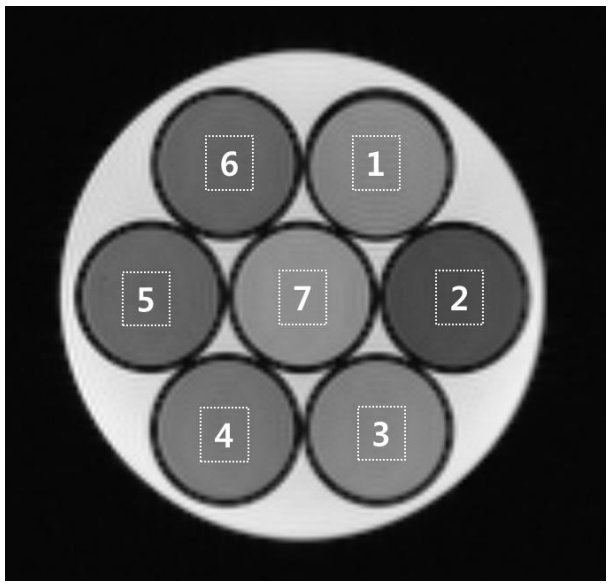

Figure 14. Development of phantom. T_2-weighted fast spin echo image of the seven-tube phantom used in this study. Tube 1 was filled with oil and tubes [2~7] were doped with varying concentrations of $GdCl_3$ (as a T_1-relaxation modifier) and agarose (as a T_2-relaxation modifier).

2.2.3. Scan parameter

The Multi-contrast sequence was designed to acquire the following imaging parameters: FOV = 256x256 *mm*2, resolution = 1.0x1.0 *mm*2 slice thickness = 5 mm, and number of slices =20. To achieve these imaging parameters, the sequence timing was set to $TR/T_{recovery}/TI$ = 10500/4250/2000 *ms,* $TE_{eff,short}/TE_{eff,long}$ = 7.9/86.9 *ms,* matrix = 256x256. The scan time of Multi-contrast sequence was 5:36 *s*.

For comparison, conventional sequences for individual contrast were acquired using the following parameters: PD images using FSE with TR/TE = 2800/9.6 *ms,* T_1-weighted images using SE with TR/TE = 650/9.6 *ms,* T_2-weighted images using FSE with TR/TE=4250/86.9 *ms* and FLAIR images using IR-FSE with TR/TE/TI = 7500/86.9/2500 *ms.* Total scan time of conventional sequences for the four contrasts was 10:32 *s*. The scan time of each sequence is summarized in Table 2. All scans were done at 3T with a local IRB approval.

Table 2. Comparison of scan time

	Conventional sequences				Multi-contrast sequence
	T_1-w (SE)	T_2-w (FSE)	PD (FSE)	FLAIR (IR)	
TR [ms]	650	4250	2800	7500	10500
ETL	1	8	8	8	8
TA [sec]	166.4	136	89.6	240	336
Total time	10 min. 32 sec.				5 min. 36 sec.

2.3. Results

2.3.1. Phantom study

Figure 15 and Figure 16 show the measured T_1 and T_2 values for the seven-tube phantom by fitting each pixel in the corresponding echo time of magnitude images to an exponential decay curve. Relaxation time maps and bar graph derived from reference sequences and proposed sequence shows similar results. Especially, T_1 and T_2 values of tubes #5 and #6 are consistent across two different spatial locations within the coil.

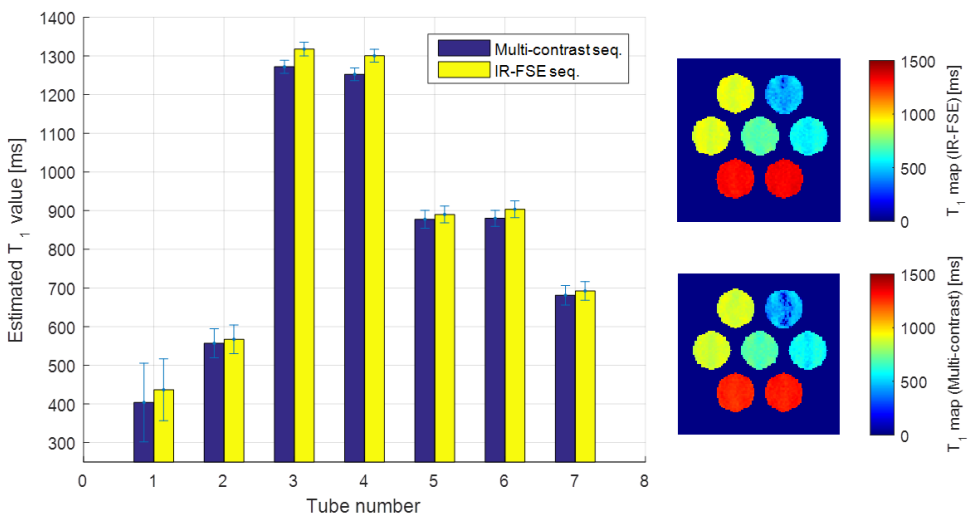

Figure 15. T_1 maps of phantom image. Two maps derived from the data of reference sequence (IR-FSE) and Multi-contrast sequence show comparable result.

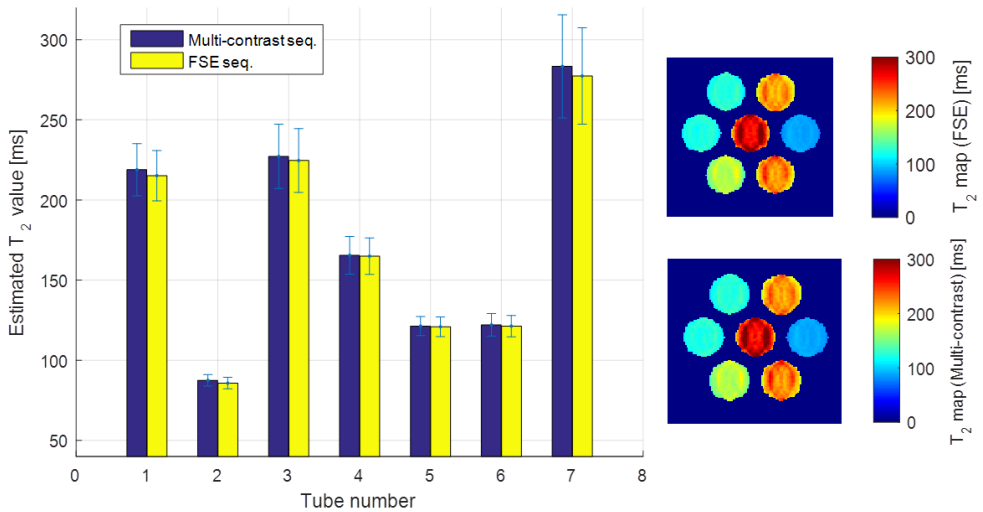

Figure 16. T_2 maps of phantom image. Two maps derived from the data of reference sequence (FSE) and Multi-contrast sequence show similar result.

2.3.2. In Vivo study

Figure 17 and Figure 18 compare in vivo test results of the four different contrasts from the reference scans with the conventional sequences and the single scan with the proposed sequence. The images from Multi-contrast sequence show similar contrasts to conventional images, while yielding a scan time reduction of 50%. The comparison of SNR in each contrast is summarized in Table 3. SNR of images was calculated according to the method defined in the NEMA [37] document. In NEMA, SNR is determined by the ratio of signal intensity to noise standard deviation. Signal intensity and noise standard deviation was measured from region of interest (ROI) and noise measurement region of interest (NMROI) respectively. NMROI should be carefully selected in the area where no the phantom and any visible artifacts exists.

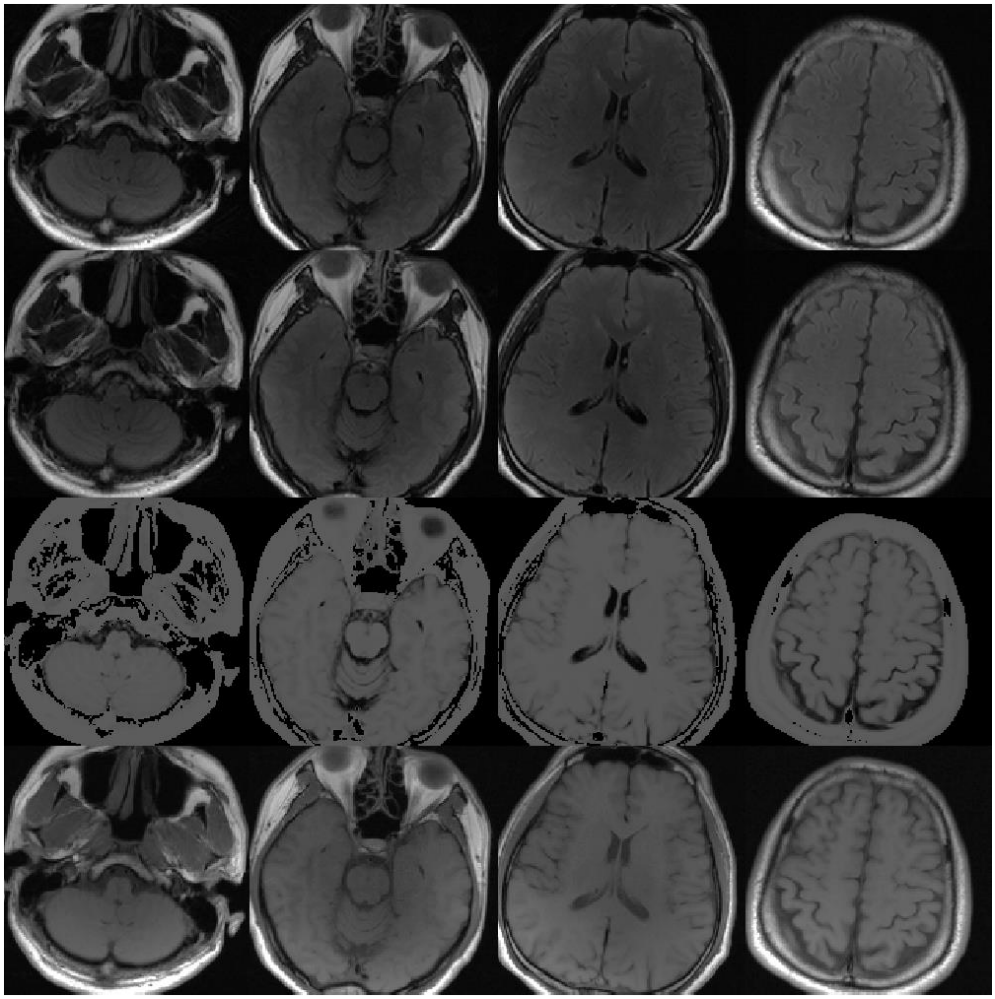

Figure 17. Comparison of images. The images in the first row are T_2-FLAIR with Multi-contrast sequence and the images in the second row are T_2-FLAIR with conventional FLAIR sequence. The images in the third row are T_1-weighted images with Multi-contrast sequence and the images in the last row are T_1-weighted with conventional SE sequence.

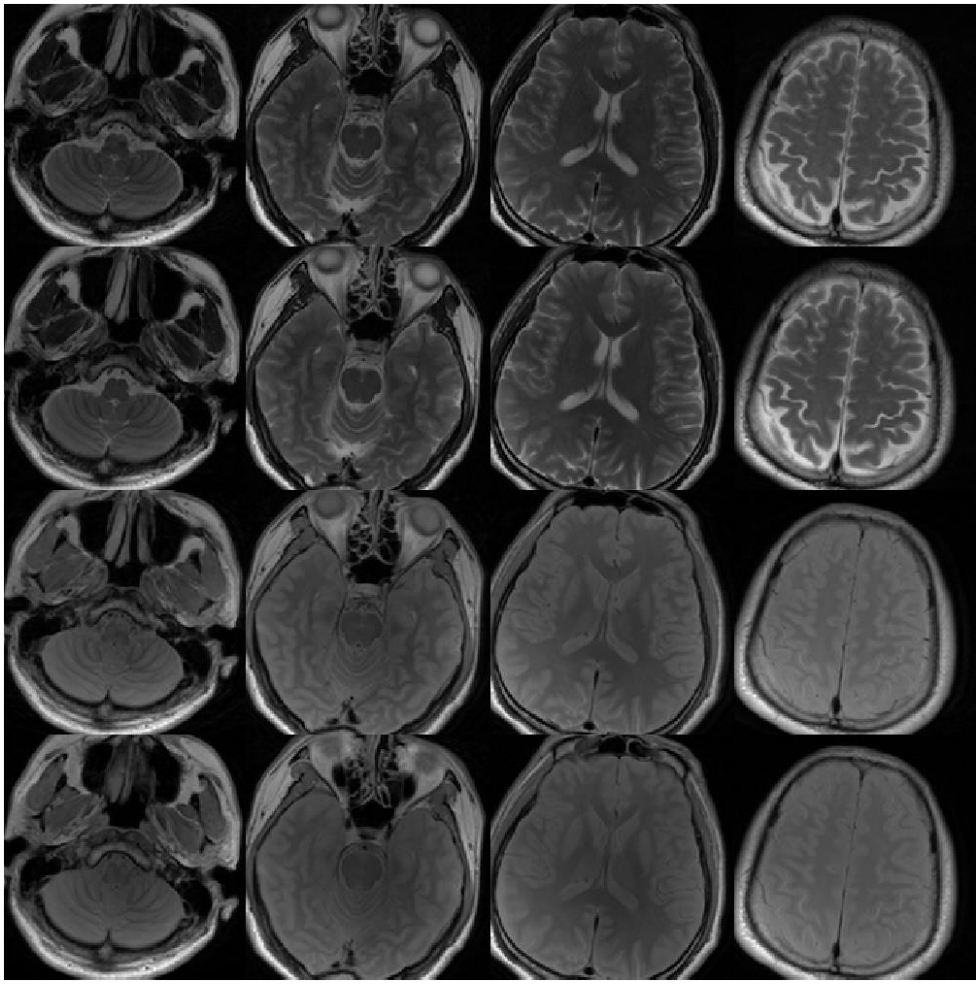

Figure 18. Comparison of images. The images in the first row are T_2-weighted images with Multi-contrast sequence and the images in the second row are T_2-weighted images with conventional FSE sequence. The images in the third row are PD images with Multi-contrast sequence and the images in the last row are PD images with conventional FSE sequence.

Table 3. Comparison of SNR of in vivo images

Contrast	Pulse sequence	White matter	Gray matter	Noise std
PD	Conventional	139.27	260.34	14.39
	Multi-contrast	129.99	244.95	16.54
T_2-weighted	Conventional	63.2	148.25	20.31
	Multi-contrast	63.94	132.53	22.9
FLAIR	Conventional	59.21	118.79	20.45
	Multi-contrast	53.86	97.64	22.64

The proposed sequence provides not only relaxation weighted images but also T_1 and T_2 maps as shown in Figure 19 and Figure 20 which add important values. Both T_1 and T_2 maps were processed by fitting algorithm using custom-written software developed in Matlab (release 2015b, MathWorks). For T_1 maps, PD images and PD-FLAIR images are used and non-linear least square fitting is performed. The signal evolution of PD images is expressed as equation (2.17) and the signal evolution of PD-FLAIR images over time is expressed as equation (2.18). So, T_1 maps are fitted so that the difference between expected the signal intensity from each equation and the measured signal intensity is minimized.

$$S_{PD} = \rho(1 - e^{-T_{recovery}/T_1}) \qquad (2.17)$$

$$S_{PD-FLAIR} = \rho(1 - 2e^{-TI/T_1} + e^{-T_{recovery}/T_1}e^{-TI/T_1}) \qquad (2.18)$$

For T_2 maps, PD images and T_2-weighted images are used. The fitting is performed using mono-exponential curve fitting and extended phase graph (EPG) dictionary fitting and the two results are compared. EPG dictionary has T_2 value range of 0.1 *ms* resolution from 1 *ms* to 300 *ms* and number of echo is 12. During the generation of EPG dictionary, T_1 value was assumed as 1000 *ms* and flip angle was set to 170° . The estimated T_2 maps using mono-exponential curve fitting show slightly over-estimated values which may originate from the stimulated echo in FSE. However, T_2 maps using EPG dictionary fitting show slightly improved values because the effect of stimulated echo was eliminated. From the third row of Figure 20, the difference between the two maps is about 5 *ms*. The difference maps are the result of subtracting T_2 maps using exponential fitting from T_2 maps using EPG dictionary fitting.

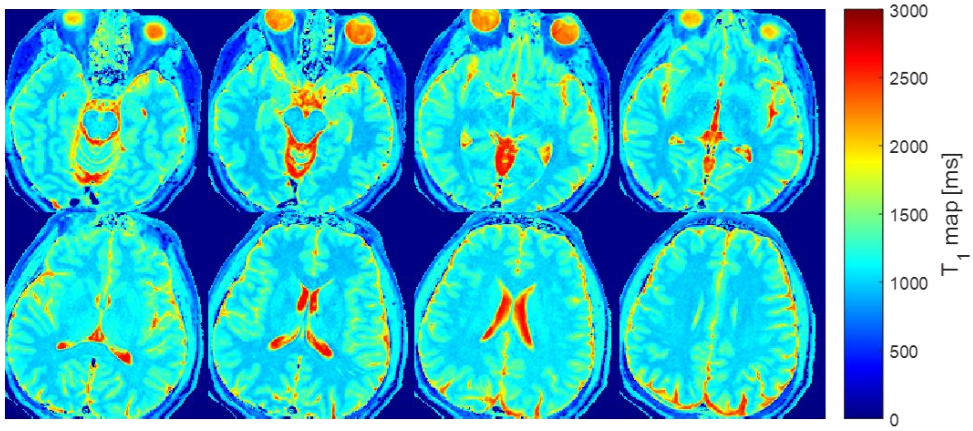

Figure 19. T_1 maps of in vivo image. Non-linear least square fitting algorithm was used.

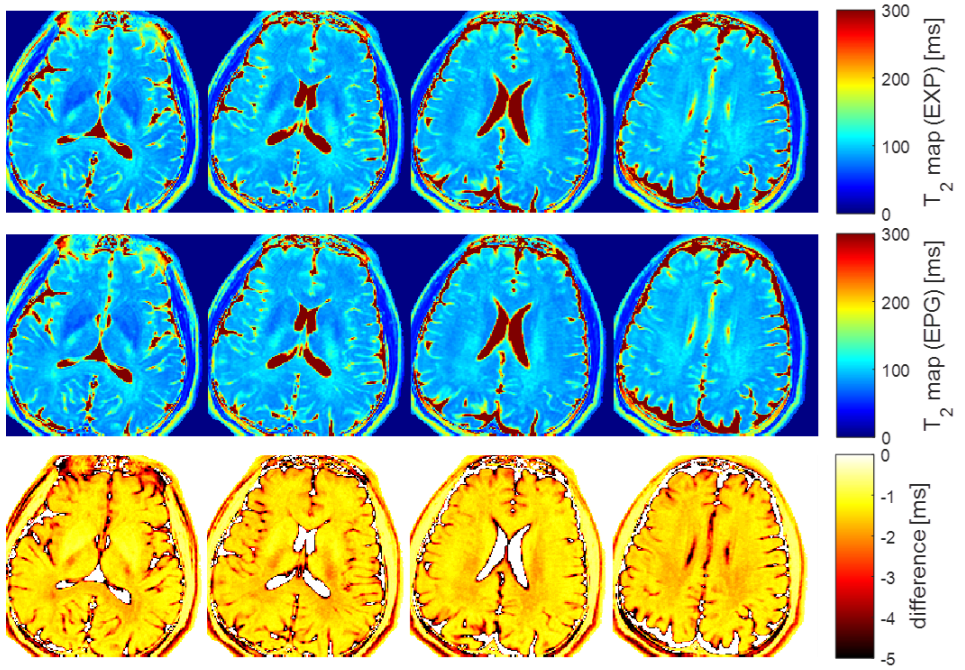

Figure 20. T_2 maps of in vivo image. The first row represents T_2 maps using exponential fitting and the second row represents T_2 maps using EPG fitting. The third row represents the different between two T_2 maps. The difference maps are the result of subtracting T_2 maps using exponential fitting from T_2 maps using EPG dictionary fitting.

2.4. Discussion and Conclusion

In this work, we introduced Multi-contrast pulse sequence for simultaneous acquisition of the four contrast images; PD, T_1-weighted, T_2-weighted and FLAIR images. The image contrast of proposed sequence is comparable to that of conventional sequences. The results demonstrate the effectiveness of our approach for multi-contrast brain imaging. The four contrasts obtained using the proposed sequence are a basic protocol commonly used in clinical practice, and it is noteworthy that shortening the acquisition time of these images contributes to dramatically shortening the diagnostic time. Directly obtained contrasts from the Multi-contrast sequence were PD, PD-FLAIR, T_2-weighted, and T_2-FLAIR and T_1-weighted contrast was synthesized from PD and PD-FLAIR images. It is also important to note that the generated T_1-weighted image of proposed sequence was free of bias field and therefore the tissue segmentation and image quality was improved compare to the conventional T_1-weighted image of spin-echo sequence. Additionally, T_1 and T_2 maps were generated at no cost providing additional benefits. Compared with other techniques for extracting tissue parameters and synthesizing images, Multi-contrast sequence has a remarkable advantage to provide naturally scanned images and quantitative maps simultaneously for diagnosis. Because tissue parameter estimation technologies such as MRF or MAGiC commonly adopt random sampling, they cannot provide natural images for diagnosis. Also, they require a large size dictionary to fit T_1 and T_2 maps from random data. It takes a long time to generate a dictionary and there is still a partial volume effect problem that cannot be addressed by the dictionary mapping methods. Especially FLAIR image is one of the images which are difficult to produce good quality image if the T_1 and T_2 values are not correct. The proposed sequence produces four contrast scanned images including FLAIR and also provides T_1 and T_2 maps at no cost. Because multi-contrast images from the proposed sequence are co-registered between different contrasts, our approach would be

beneficial for investigation of pathophysiological mechanisms such as the studies introduced in [30]. Hence, the method may have potential applications as a fast evaluation tool for clinical scans.

While the proposed Multi-contrast sequence has several advantages, there are some points to be improved. For T_2 maps, simple EPG fitting was performed but the accuracy of mapping result may be improved by using advanced EPG fitting algorithm like slice profile resolved EPG (SEPG) [38] or Bloch simulation. Recently, the advanced fitting algorithms are introduced by reflecting slice profile and B_1 maps into the fitting model. As for the phase encoding order of shared echoes in DE-FSE data acquisition unit, it may be necessary to find an optimal order for both images with short TE and long TE in the future. In the experiment of phantom and in vivo studies, the phase encoding order of shared echoes is designed to be optimized for T_2-weighted images with long TE, but no visible artifact was found in the images with short TE of experimental results. If we compare the point spread function according to various phase encoding orders and find the optimal one for both images with short TE and long TE, we can improve the image quality more.

3. Conclusion

MRI is an important imaging modality that plays an essential role in the pathological diagnosis and diagnosis of disease. Compared to some other imaging methods like CT or X-rays, one of the advantages of MRI is that it uses non-ionizing radiation, and thus it poses minimal risk on human body. By changing the pulse sequences and the parameter of protocols of MR scanner, images with different contrasts can be obtained.

However, the main challenge of MRI is the acquisition speed, which limits the clinical application of MRI. If the scan time is long, it causes inconvenience to the patients who feel frustration due to the closed feeling in the bore. In the case of abdominal images in which motion artifacts frequently occur due to the patient's breathing, a high-speed imaging technique is desperately needed because the user can scan only while the patient is holding to breath in order to obtain a satisfactory quality image. In addition, there is a problem in that an infant or a cognitive impairment patient who are unable to communicate or control their movements, and therefore, the scan is only possible under an anesthesia. On the other hand, like T_1 maps and T_2 maps, the quantitative maps showing the characteristics of the tissues provide valuable information in monitoring of the change of the patient's condition, but long scan time is required because repeated scans with various parameters are required.

This thesis proposes Multi-contrast pulse sequence in order to accelerate MRI while preserving the image quality. The goal of Multi-contrast sequence is to provide not only a quantitative maps but also diagnosis ready images of the comparable level as the images from the conventional imaging sequences. We developed novel pulse sequence for simultaneous acquisition of the four contrast images. Experimental results of phantom and in vivo scans show satisfactory image quality.

The main contributions of this work include:

1. The development of rapid evaluation tool. The Multi-contrast sequence not only produces clinically useful images, also achieves minimalistic scan times. The scan time required to obtain four contrast images has been reduced to about half compared to the scan time of the existing sequences.
2. The development of fast quantification tool. The Multi-contrast sequence generates co-registered images with multi-point TE and TR and provides quantitative maps, T_1 and T_2 maps, at no cost.

The new pulse sequence in this thesis will be a small step in extending the use of MRI. As explained in the previous discussion, applicable technologies are being introduced to improve the performance of this approach. The future directions of this work include improvement of the accuracy of the fitting algorithm in relaxation time mapping based on images from Multi-contrast pulse sequence.

Bibliography

[1] Z. P. Liang and P. C. Lauterbur. Principles of Magnetic Resonance Imaging: a signal processing perspective. Wiley-IEEE Press, 1 edition, 1999.

[2] Bloch F, Hansen WW, Packard ME. Nuclear induction. Phys Rev 1946; 69:127.

[3] E.L. Hahn, "Spin echoes", Physical Review, vol. 80, p. 580, 1950.

[4] R.V. Damadian. Tumor detection by nuclear magnetic resonance. Science, 171:1151-1153, 1971.

[5] Greg J. Stanisz, Ewa E. Odrobina, et al. "T1, T2 Relaxation and Magnetization Transfer in Tissue at 3T," Magn. Reson. Med., 54:507-512, 2005.

[6] Matt A. Bernstein, Kevin F. King, Xiaohong Joe Zhou. Handbook of MRI Pulse Sequences. Elsevier Academic Press, p. 611-616.

[7] S. Meiboom & D. Gill, "Modified spin-echo method for measuring nuclear relaxation times", Review of Scientific Instruments, vol. 29, p. 688, 1958.

[8] Feinberg DA, Hale JD, Watts JC, et al. Halving MR imaging time by conjugation: demonstration at 3.5 kG. Radiology 161:527-531, 1986.

[9] J. R. MacFall, N. J. Pelc, and R. M. Vavrek, "Correction of spatially dependent phase shifts for partial Fourier imaging," Magn. Reson. Imag.,vol. 6, pp. 143-155, 1988.

[10] K. P. Pruessmann, M. Weiger, M. B. Scheidegger, and P. Boesiger, "SENSE: Sensitivity encoding for fast MRI," Magn. Reson. Med., vol. 42, pp. 952-962, 1999.

[11] D. K. Sodickson and W. J. Manning, "Simultaneous acquisition of spatial harmonics (SMASH): Fast imaging with radiofrequency coil arrays," Magn. Reson. Med., vol. 38, pp. 591-603, 1997.

[12] Griswold MA, Jakob PM, Nittka M, Goldfarb JW, Haase A. Partially parallel imaging with localized sensitivities (PILS). Magn Reson Med 2000;44:602-609.

[13] Griswold MA, Jakob PM, Heidemann RM, Nittka M, Jellus V, Wang J, Kiefer B, Haase A. Generalized autocalibrating partially parallel acquisitions (GRAPPA). Magn Reson Med 2002;47:1202--1210.

[14] Lauterbur P. Image formation by induced local interactions: examples employing nuclear magnetic resonance. Nature 1973;242:190-191.

[15] Glover GH, Pauly JM. Projection reconstruction techniques for reduction of motion effects in MRI. Magn Reson Med 1992;28:275-289.

[16] Ahn CB, Kim JH, Cho ZH. High-speed spiral-scan echo planar NMR imaging-I. IEEE Trans Med Imaging 1986;5:2-7.

[17] Meyer CH, Hu BS, Nishimura DG, Macovski A. Fast spiral coro-nary artery imaging. Magn Reson Med 1992;28:202-213.

[18] Donoho DL. Compressed sensing. IEEE Trans on Inform Theory 2006;52:1289-1306.

[19] Lustig M, Donoho DL, Pauly JM. Sparse MRI: The application of com-pressed sensing for rapid MR imaging. Magn Reson Med 2007;58:1182-1195.

[20] Blake A. Johnson, Evan K. Fram, et al. Evaluation of Shared-View Acquisition Using Repeated Echoes (SHARE): A Dual-Echo Fast Spin-Echo MR Technique. Am J Neuroradiology 15:667-673, Apr 1994.

[21] Ralf Mekle, Andrew F. Laine, et al. Combined MR Data Acquisition of Multicontrast Images Using Variable Acquisition Parameters and K-Space Data Sharing. IEEE Transactions of Medical Imaging, Vol. 22, No. 7, July 2003.

[22] D. A. Feinberg, B. Kiefer, and A. W. Litt, "Dual contrast GRASE (gradient-spin echo) imaging using mixed bandwidth," Magn. Reson. Med.,vol. 31, pp. 461-464, 1994.

[23] Koichi Oshio and Ference A. Jolesz. Simultaneous Acquisition of Proton Density, T_1 and T_2 Images with Triple Contrast RARE Sequence. Journal of Computer Assisted Tomography 17 (2):333–338, March/April, 1993.

[24] Fuchs K, Hezel F, Klix S, Mekle R, Wuerfel J, Niendorf T. Simultaneous dual contrast weighting using double echo rapid acquisition with relaxation enhancement (RARE) imaging. Magn. Reson. Med. 2014;72:1590–1598.

[25] Kazuhiro Takeo, Akihiro Ishikawa, et al. FASCINATE: A Pulse Sequence for Simultaneous Acquisition of T_2–Weighted and Fluid–Attenuated Images. Magnetic Resonance in Medicine 51:205–211, 2004.

[26] F. G. Woermann, H. Steiner, G. J. Barker, P. A. Bartlett, C. E. Elger, J. S. Duncan, and M. R. Symms, "A fast FLAIR dual–echo technique for hippocampal T_2 relaxometry: First experiences in patients with temporal lobe epilepsy," J. Magn. Reson. Imag., vol. 13, pp. 547–552, 2001.

[27] Jaeseok Park, Suhyung Park, et al. Phase–Sensitive, Dual–Acquisition, Single–Slab, 3D, Turbo–Spin–Echo Pulse Sequence for Simultaneous T_2–weighted and Fluid–Attenuated Whole–Brain Imaging. Magnetic Resonance in Medicine 63:1422–1430, 2010.

[28] Jonathan I. Tamir, Martin Uecker, et al. T_2 Shuffling: Sharp, Multicontrast, Volumetric Fast Spin–Echo Imaging. Magnetic Resonance in Medicine 77:180–195, 2017.

[29] Marques, J.P., Kober, T., Krueger, G., van der Zwaag, W., Van de Moortele, P.F., Gruetter, R.. MP2RAGE, a self bias–field corrected sequence for improved segmentation and T_1–mapping at high field. NeuroImage 49, 1271–1281, 2010.

[30] C. Granziera, A. Daducci, et al. A multi–contrast MRI study of microstructural brain damage in patients with mild cognitive impairment. NeuroImage: Clinical 8, 631–639, 2015.

[31] J Hennig, Multiecho Imaging Sequences with Low Refocusing Flip Angles. Journal of Magnetic Resonance 78, 397–407, 1988.

[32] Ma, D., Gulani, V., Seiberlich, N., Liu, K., Sunshine, J., Duerk,

J., Griswold,M., Magnetic resonance fingerprinting. Nature 14 (495(7440)), 187-192, 2013.

[33] Hernan Jara, Arnaud Guidon, et al. Quadra-FSE: A Multi-Platform Pulse Sequence for Multispectral qMRI (PD, T_1, T_2). In: Proc 24th Annual Meeting ISMRM, Singapore, 2016. p 1817.

[34] Park HW, Cho MH, Cho ZH. Time-multiplexed multislice inversionrecovery techniques for NMR imaging. Magn Reson Med 1985;2:534-539.

[35] Sean C.L. Deoni, Brian K. Rutt, et al. Gleaning Multicomponent T_1 and T_2 Information From Steady-State Imaging Data. Magn Reson Med 60, 1372-1387, 2008.

[36] H.Y. Carr & E.M. Purcell, "Effects of diffusion on free precession in nuclear magnetic resonance experiments", Physical Review, vol. 94, no. 3, pp. 630-638, 1954.

[37] NEMA Standards Publication MS 1-2008. National Electrical Manufacturers Association.

[38] R. Marc Lebel and Alan H. Wilman. "Transverse Relaxometry with Stimulated Echo Compensation",

초 록

다중 컨트라스트 영상기법: Proton density, T_1, T_2 및 FLAIR 영상을 동시에 획득하는 펄스시퀀스

정 진 희

전기정보공학부

서울대학교 대학원

자기공명영상장치(MRI)는 광범위하게 사용되는 비침습적인 기법의 의료영상 장치이다. X-ray나 컴퓨터 단층 촬영(CT)과 같은 다른 의료영상기법과 달리, MRI는 검사과정에서 방사선의 영향을 받지 않는 것이 장점이다. 또한, MRI는 다양한 펄스시퀀스와 프로토콜을 활용하여 다중 컨트라스트 영상을 제공하여 진단에 도움을 준다. 그러나, 영상의 획득 속도가 느린 단점이 있어 다양한 어플리케이션에 활용되지 못하는 제약이 있다. 이러한 MRI의 영상획득 속도 문제를 해결하기 위해서, 다중 컨트라스트 영상을 하나의 펄스시퀀스를 통해 동시에 얻는 영상기법을 개발하였다. 다중 컨트라스트 시퀀스라는 새로운 펄스 시퀀스는 PD (proton density), T_1, T_2 and FLAIR 4종류의 컨트라스트 영상을 6분 이내의 싱글 시퀀스로 제공한다. 기존의 펄스 시퀀스를 이용한 스캔시간과 비교하면, 약 50%의 스캔시간을 단축한 것이다. 또한, 제안된 시퀀스로 획득한 영상을 이용하여, T_1 및 T_2 map을 생성할 수 있다. 제안된 시퀀스의 효과를 입증하기 위해서, 팬텀 및 in vivo 실험을 진행하였다. 다중 컨트라스트 시퀀스는 향후 신속한 진단도구로서 활용될 수 있다.

주요어: 자기공명영상, 다중 컨트라스트, 터보 스핀에코, FLAIR 영상, 정량적 영상

학 번: 2015-20990